

Anisotropy Analysis of Turbulent Swirl Flow

Darko R. Radenković

Teaching Assistant
University of Belgrade
Faculty of Mechanical Engineering

Jela M. Burazer

PhD Student
University of Belgrade
Faculty of Mechanical Engineering

Dorđe M. Novković

Teaching Assistant
University of Priština
Faculty of Technical Sciences

Anisotropy invariant map proposed by Lumley and Newman and barycentric map proposed by Banerjee et al. were used in order to estimate the degree of anisotropy in turbulent swirl flow. The differences in visual interpretations of anisotropy states in these two maps were analysed and mathematical basis of these two maps was derived. Experimental data reveal that there is significant influence of swirl on the anisotropy of turbulence. Anisotropy invariant mapping shows that different flow regions of swirl flow are characterized by different anisotropy states.

Keywords: anisotropy, anisotropy invariant map, barycentric map, swirl, turbulence.

1. INTRODUCTION

From a computational point of view, it is of considerable interest to have some knowledge about the expected anisotropy in the flow field [1]. The modelling of the Reynolds stress anisotropy tensor is the most important and delicate element in the Reynolds stress model, where the knowledge of the departure from isotropy is essential. In [2] and [3] the anisotropy of turbulent flow was analysed. Useful tools to quantify the degree of anisotropy in turbulent flows are anisotropy invariant maps. These maps represent a domain within which all realisable Reynolds stress invariants must lie. In current work, two representations of these maps are used: anisotropy invariant map (AIM) which is a representation proposed by Lumley and Newman [4] and a barycentric map (BM), a representation proposed by Banerjee et al. [5]. In this paper, the anisotropy analyses is conducted using these two maps in case of a swirl flow.

Swirl flows are an important class of flows, common in nature and in many technical applications. These highly complex flows have been studied for a long time, but the modelling and understanding of such flows still represents a challenge to turbulence modellers.

Tangential velocity distributions from experimental investigations of swirl flows showed that there are four regions in the flow: vortex core, shear vortex layer, main flow and wall region [6]. Each of these regions has important properties and their existence makes physical-mathematical modelling of such flows very complicated. Experimental results from a great number of experimental studies demonstrated that swirl decayed with axial distance.

Negative eddy viscosities were observed in certain parts of swirl flow [7]. Obviously, standard two-equation model cannot successfully predict these flows. The reason is that swirl flow is characterized by anisotropy in eddy viscosity in contrast to two-equation

model of turbulence, which assumes the eddy viscosity to be isotropic. Reynolds stress model is suggested in order to predict turbulence in swirl flow field successfully [8]. The motivation for the development of the Reynolds stress model is the inability of any eddy-viscosity model to allow a non-local relationship between Reynolds stress tensor and mean strain rate tensor, that is, history effects.

The aim of this paper is to present and analyse part of experimental results from [9] in order to improve our knowledge of the anisotropy in swirl flow. The AIM and BM were used in order to obtain easier understanding of swirl influence on the anisotropy of turbulence. Mathematical basis of both maps are explained in the paper. Differences between these two maps were analysed in order to determine which map gives better graphical result.

2. SWIRL FLOW PROPERTIES

Radial distributions of mean velocity components and terms of Reynolds stress tensor are presented in this section. Measurements of these quantities were carried out in 12 appropriately selected points in one cross section of a straight circular pipe. More details about experiment can be found in [9].

2.1 Mean velocity distribution

Profiles of tangential mean and axial mean velocities are plotted in Figure 1. These velocities are normalized with bulk velocity U_m . Radial velocity component is negligible and this velocity profile is not shown.

As it is said earlier, there are four characteristic regions within the swirling flow. These regions have important structural and statistical properties.

Vortex core is characterized by linear variation of the tangential velocity component with radial distance from the pipe centreline. Vortex core, for the velocity profile plotted in Figure 1, extends up to $r/R \approx 0.23$. Shear flow region is characterized by weak tangential velocity variation. It extends approximately between $0.23 < r/R < 0.56$ for velocity profile shown in Figure 1. Mean flow region is characterized with free vortex distribution. For considered velocity profile beginning

Received: March 2013, Accepted: November 2013

Correspondence to: Darko R. Radenković
Faculty of Mechanical Engineering,
Kraljice Marije 16, 11120 Belgrade 35, Serbia
E-mail: dradenkovic@mas.bg.ac.rs

doi:10.5937/fmet1401019R

© Faculty of Mechanical Engineering, Belgrade. All rights reserved

FME Transactions (2014) 42, 19-25

19

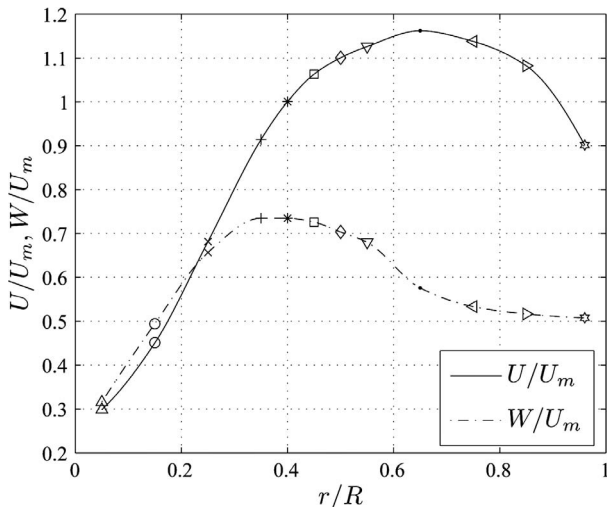


Figure 1. Normalized mean velocity profiles

of this region is defined at $r/R \approx 0.56$. Near the wall, tangential velocity distribution reaches zero very rapidly. Measurements could not be made near the wall and due to this fact, end of the mean flow region i.e. beginning of the wall region is not specified for the velocity profile from Figure 1.

2.2 Reynolds stresses distributions

Radial distributions of turbulence intensities normalized with bulk velocity U_m are shown in Figure 2. These distributions have similar profiles. Turbulence intensities are in range from 8 to 27 percent of the bulk velocity U_m .

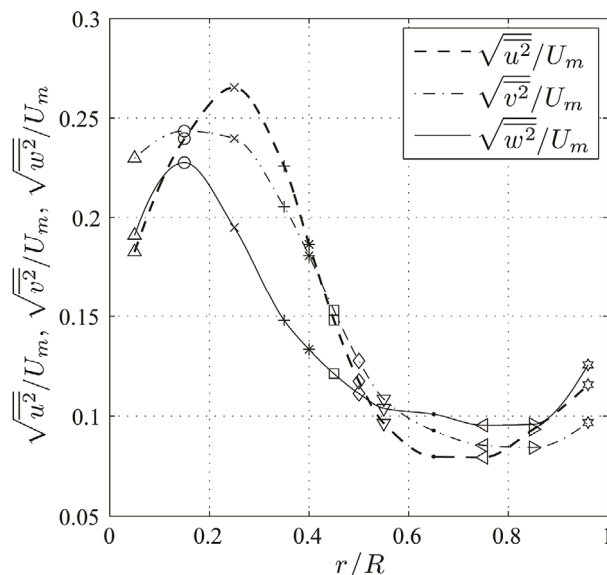


Figure 2. Normalized distributions of turbulence intensities

Turbulent shear stresses distributions over cross section are presented in Figure 3. These distributions do not have similar profiles in contrast to distributions of turbulence intensities shown in Figure 2. Reynolds stress component \overline{uv} has negative values in region $0.05 < r/R < 0.62$ and a small positive value in region $0.62 < r/R < 0.96$. The component \overline{vw} is positive

through the range in which the measurements are performed. The Reynolds stress \overline{uw} is positive in the region $0.05 < r/R < 0.38$, negative for $0.38 < r/R < 0.7$ and negligible for $0.7 < r/R < 0.96$.

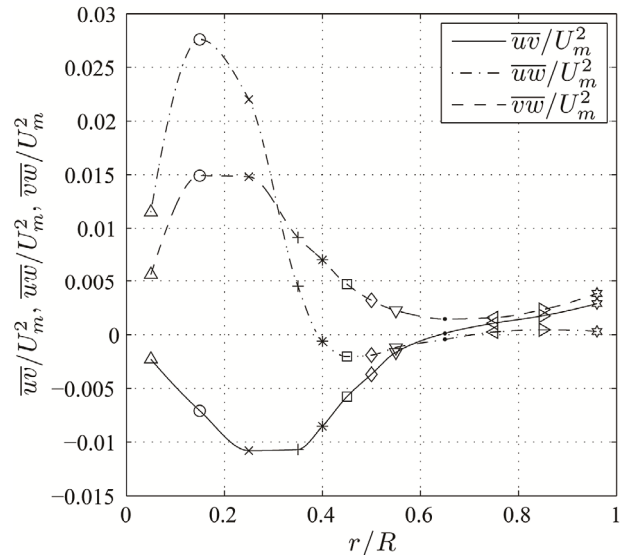


Figure 3. Normalized profiles of off-diagonal components of the Reynolds stress tensor

There is a big interaction between mean and fluctuating velocity field. This interaction causes the highly complex flow field.

3. REPRESENTATION OF ANISOTROPY IN TURBULENCE

The Reynolds stress tensor is a symmetric second-order tensor, given by

$$\underline{\underline{T}} = \tau_{ij} = \begin{pmatrix} \overline{u^2} & \overline{uv} & \overline{uw} \\ \overline{vu} & \overline{v^2} & \overline{vw} \\ \overline{wu} & \overline{wv} & \overline{w^2} \end{pmatrix}$$

It is useful to decompose this tensor into the sum of its deviator (traceless tensor), τ'_{ij} and a spherical (isotropic) tensor, τ°_{ij} , as follows:

$$\tau_{ij} = \tau^{\circ}_{ij} + \tau'_{ij}$$

The spherical part is defined as

$$\tau^{\circ}_{ij} = \frac{1}{3} \tau_{kk} \delta_{ij} = \frac{1}{3} q^2 \delta_{ij}$$

where q^2 represents the trace of the Reynolds stress tensor and it is equal to twice the kinetic energy of turbulence $q^2 = 2k$.

The deviator is now expressed as

$$\tau'_{ij} = \tau_{ij} - \frac{1}{3} \tau_{kk} \delta_{ij} = \overline{u_i u_j} - \frac{1}{3} q^2 \delta_{ij}$$

When the deviator τ'_{ij} is normalised with the trace of Reynolds stress tensor q^2 , the anisotropy tensor $\underline{\underline{A}} = a_{ij}$ is obtained as follows [4]

$$a_{ij} = \frac{\tau'_{ij}}{q^2} = \frac{\overline{u_i u_j}}{q^2} - \frac{1}{3} \delta_{ij}. \quad (1)$$

It isolates the property of anisotropy of Reynolds stress tensor from other flow properties. The anisotropy tensor is dimensionless, has zero trace and in the case of isotropy it vanishes identically.

Having in mind that the anisotropy tensor is symmetric, i.e. $a_{ij} = a_{ji}$, it is possible to find an orthonormal basis $\{\underline{n}_1, \underline{n}_2, \underline{n}_3\}$ such that:

$$\underline{\underline{A}} = \lambda_i \underline{n}_i \underline{n}_i,$$

or in matrix form

$$\underline{\underline{A}} = \begin{pmatrix} \lambda_1 & 0 & 0 \\ 0 & \lambda_2 & 0 \\ 0 & 0 & \lambda_3 \end{pmatrix}.$$

Vectors \underline{n}_i that diagonalize anisotropy tensor $\underline{\underline{A}}$ are called eigenvectors (or principal directions) and λ_i are called eigenvalues (or principal values) of anisotropy tensor $\underline{\underline{A}}$. The symmetry property of anisotropy tensor $\underline{\underline{A}}$ ensures that all three eigenvalues and the associated eigenvalues are real. The eigenvalues of anisotropy tensor $\underline{\underline{A}}$ are determined by solving the characteristic equation

$$\det(\underline{\underline{A}} - \lambda \underline{\underline{I}}) = 0 \text{ or } |a_{ij} - \lambda \delta_{ij}| = 0.$$

Evaluation of this determinant leads to a characteristic polynomial of $\underline{\underline{A}}$, which is given by

$$\lambda^3 - I_1 \lambda^2 + I_2 \lambda - I_3 = 0, \quad (2)$$

where

$$\begin{aligned} I_1 &= \text{tr}(\underline{\underline{A}}) = a_{kk}, \\ I_2 &= \frac{1}{2} [(\text{tr} \underline{\underline{A}})^2 - \text{tr} \underline{\underline{A}}^2] = \frac{1}{2} (a_{ii} a_{jj} - a_{ij} a_{ji}) \text{ and} \\ I_3 &= \det(\underline{\underline{A}}) = \frac{1}{3} (a_{ii} a_{jj} a_{kk} - 3 a_{ii} a_{jj}^2 + a_{ii}^3). \end{aligned}$$

The scalar coefficients I_1 , I_2 and I_3 are called the first, second and third invariant of $\underline{\underline{A}}$. With respect to (1), it is clear that the first invariant I_1 is equal to zero, and the second and third invariant are reduced to:

$$\begin{aligned} I_2 &= -\frac{1}{2} \text{tr} \underline{\underline{A}}^2 = -\frac{1}{2} a_{ij} a_{ji} \text{ and} \\ I_3 &= \frac{1}{3} \text{tr} \underline{\underline{A}}^3 = \frac{1}{3} a_{ij} a_{jk} a_{ki}. \end{aligned}$$

Instead of the second and third invariant, I_2 and I_3 , the turbulence state is analysed with invariants II_a and III_a which differ from former invariants by only a numerical factor as follows

$$\begin{aligned} II_a &= -2I_2 = a_{ij} a_{ji} \text{ and} \\ III_a &= 3I_3 = a_{ij} a_{jk} a_{ki}. \end{aligned}$$

A cross-plot of II_a versus III_a , shown in Figure 4, represents anisotropy invariant map (AIM) where II_a represents the degree of anisotropy and III_a indicates the nature of anisotropy [3].

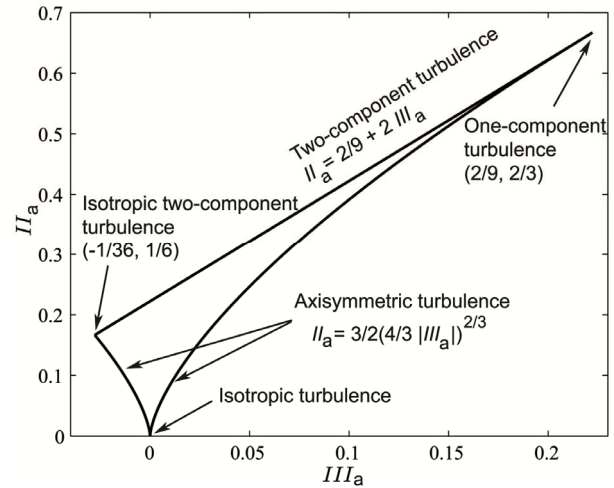


Figure 4. Anisotropy invariant map (AIM)

Characteristic states of turbulence are represented by the boundaries of this map. There are two curves extending from the origin. Right curve ($II_a = \frac{3}{2} \left(\frac{4}{3} III_a \right)^{2/3}$) corresponds to axisymmetric expansion in which one diagonal component of Reynolds stress tensor is larger than the other two, equal components. The left curve ($II_a = \frac{3}{2} \left(-\frac{4}{3} III_a \right)^{2/3}$) represents an axisymmetric contraction in which one component is smaller than the other two components, which are equal.

Limiting points at the end of these curves are important: isotropic turbulence at the origin (0,0), isotropic two-component turbulence $\left(-\frac{1}{36}, \frac{1}{6} \right)$ at the end of the left curve and one-component turbulence $\left(\frac{2}{9}, \frac{2}{3} \right)$ at the end of right curve. Upper boundary line of the AIM represents the two-component turbulence ($II_a = \frac{2}{9} + 2 III_a$) which is reached near the solid walls where the wall-normal component of the fluctuations vanishes much faster than the other components [8]. Anisotropy invariants (II_a, III_a) are nonlinear functions of Reynolds stress tensor components which is the main flaw of this concept.

Another way to visualize the anisotropy of the turbulence is using a barycentric map (BM). The

anisotropy states in this map are linear functions of the Reynolds stresses. The BM is shown in Figure 5.

The turbulence state in BM is characterised by reorganised anisotropy tensor $\underline{\underline{A}}^r$ that can be written in the matrix form as

$$\underline{\underline{A}}^r = \begin{pmatrix} \lambda_1 & 0 & 0 \\ 0 & \lambda_2 & 0 \\ 0 & 0 & \lambda_3 \end{pmatrix},$$

where the eigenvalues λ_1 , λ_2 and λ_3 are sorted in decreasing order, i.e. $\lambda_1 = \lambda_{\max}$, $\lambda_2 = \lambda_{\text{int}}$ and $\lambda_3 = \lambda_{\min}$ where λ_{\max} , λ_{int} and λ_{\min} denote maximum, intermediate and minimum value of the roots of the characteristic polynomial (2). It is straightforward to prove (with respect to (1)) that interval between which eigenvalues can be calculated is $-\frac{1}{3} \leq \lambda_i \leq \frac{2}{3}$.

The limiting states of turbulence are determined by the number of non-zero eigenvalues of tensor $\underline{\underline{A}}^r$ and by equalities between them. These limiting states are: one-component state ($\lambda_1 = \frac{2}{3}$, $\lambda_2 = \lambda_3 = -\frac{1}{3}$), two-component state ($\lambda_1 = \lambda_2 = \frac{1}{6}$, $\lambda_3 = -\frac{1}{3}$) and three-component state ($\lambda_1 = \lambda_2 = \lambda_3 = 0$). Corresponding basis matrices are

$$\underline{\underline{A}}_{1c}^r = \begin{pmatrix} 2/3 & 0 & 0 \\ 0 & -1/3 & 0 \\ 0 & 0 & -1/3 \end{pmatrix},$$

$$\underline{\underline{A}}_{2c}^r = \begin{pmatrix} 1/6 & 0 & 0 \\ 0 & 1/6 & 0 \\ 0 & 0 & -1/3 \end{pmatrix} \text{ and } \underline{\underline{A}}_{3c}^r = \begin{pmatrix} 0 & 0 & 0 \\ 0 & 0 & 0 \\ 0 & 0 & 0 \end{pmatrix}.$$

Every realisable turbulence state can be expressed as a combination of the above limiting states as

$$\underline{\underline{A}}^r = C_{1c}^a \underline{\underline{A}}_{1c}^r + C_{2c}^a \underline{\underline{A}}_{2c}^r + C_{3c}^a \underline{\underline{A}}_{3c}^r, \quad (3)$$

where:

$$\{C_{1c}^a, C_{2c}^a, C_{3c}^a\}$$

are coefficients such that

$$C_{1c}^a + C_{2c}^a + C_{3c}^a = 1,$$

and the values of these coefficients is in the range $[0, 1]$.

A value of 1 corresponds to respective limiting state and a value of 0 means that the respective limiting state is away from the observed state. Above properties are satisfied by setting the coefficients $\{C_{1c}^a, C_{2c}^a, C_{3c}^a\}$ as the functions of the eigenvalues of the tensor $\underline{\underline{A}}^r$, as follows:

$$C_{1c}^a = \lambda_1 - \lambda_2,$$

$$C_{2c}^a = 2(\lambda_2 - \lambda_3) \text{ and}$$

$$C_{3c}^a = 3\lambda_3 + 1.$$

In order to plot BM, the basis matrices $\underline{\underline{A}}_{1c}^r$, $\underline{\underline{A}}_{2c}^r$ and $\underline{\underline{A}}_{3c}^r$ are identified as the three vertices of the triangle, with coordinates (x_{1c}, y_{1c}) , (x_{2c}, y_{2c}) and (x_{3c}, y_{3c}) . The coordinates of vertices should satisfy the form of the equilateral triangle because this form does not introduce visual bias of the limiting states.

The coordinates of a new point are calculated, as an analogy to (3), as:

$$x_n = C_{1c}x_{1c} + C_{2c}x_{2c} + C_{3c}x_{3c},$$

$$y_n = C_{1c}y_{1c} + C_{2c}y_{2c} + C_{3c}y_{3c}.$$

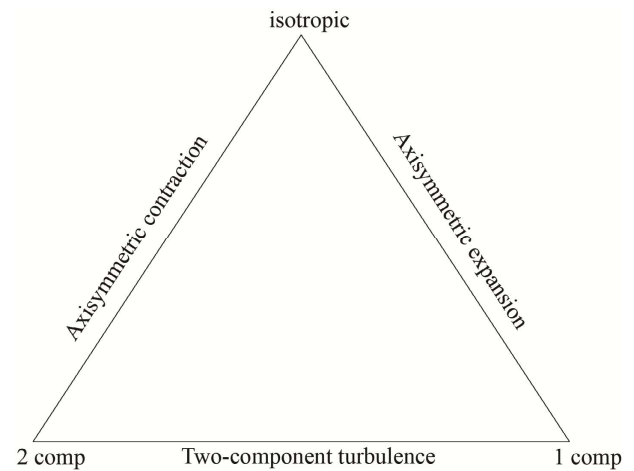


Figure 5. Barycentric map (BM)

4. INVARIANT MAPS APPLICATION IN TURBULENT SWIRL FLOW

Figure 6 shows radial distributions of components of the Reynolds stress anisotropy tensor a_{ij} . The variations in these distributions show highly complex structure of turbulence.

An important characteristic of turbulent swirl flow is distribution of anisotropy component a_{uv} . Negative values of this component in vortex core and shear flow region mean that the transfer of axial linear momentum is directed toward the pipe axis, which will result with smoother downstream velocity profile [9].

While components of anisotropy tensor a_{ij} represent the degree of anisotropy of Reynolds stress tensor components, overall anisotropy can be more clearly seen from anisotropy maps. The AIM is plotted in Figure 7, and the BM is plotted in Figure 8.

The visualisation of tensor fields improves the understanding and interpretation of tensor data. Due to that fact, the shape of Reynolds stress tensor for characteristic measuring points is given in Figure 7. The equation which defines the shape of Reynolds stress tensor is

$$\left(\frac{x}{\sigma_1}\right)^2 + \left(\frac{y}{\sigma_2}\right)^2 + \left(\frac{z}{\sigma_3}\right)^2 = 1.$$

This is an ellipsoid equation whose principal axes coincide with the stress axes and radii are equal to the absolute value of the eigenvalues $|\sigma_1|$, $|\sigma_2|$ and $|\sigma_3|$ of the Reynolds stress tensor. If the σ_1 is large and the other two eigenvalues are small but equal, $\sigma_2 = \sigma_3$, the shape of stress tensor would be prolate spheroid. On the other hand, if σ_1 is smaller than the other two eigenvalues, the shape of the stress tensor would be the oblate spheroid [10]. These observations are confirmed in Figure 7: at measuring point number 3 shape of stress tensor is oblate spheroid and this shape gradually changes toward prolate spheroid at measuring point number 7

The AIM and BM represent the same information about overall anisotropy in different ways. Anisotropy states in the AIM are nonlinear function of stresses, while anisotropy states in the BM are linear function of stresses.

For the first two measuring points, which belong to the vortex core, $r/R=0.05$ and $r/R=0.15$ anisotropy states lie close to axisymmetric contraction line in both maps, in the AIM (Figure 7) and in the BM (Figure 8). The

next six measuring points correspond to shear layer. With radius increase, corresponding invariants in the AIM, i.e. corresponding points in the BM tend toward axisymmetric expansion line.

The last four measuring points correspond to mean flow region. Corresponding data shift parallel to axisymmetric contraction line in both maps. In order to analyse the difference between the AIM and the BM, Figure 9 shows radial distribution of principal values of anisotropy tensor. Now it will be considered anisotropy state from measuring point $r/R=0.50$ (number 7 in Figures 7, 8 and 9). Figure 9 shows that this state does not represent axisymmetric expansion turbulence, since principal anisotropy tensor components λ_1 and λ_2 are not equal. Component λ_2 is 24% larger than component λ_1 . However, this state lies on axisymmetric expansion curve in the AIM (Figure 7), while it is shown a little offset from axisymmetric expansion line in the BM (Figure 8).

Another difference between the AIM and the BM is observed at $r/R=0.65$ (number 9 in Figures 7, 8 and 9). Figure 9 shows that there are significant differences between principal anisotropy tensor components λ_1 and λ_2 so this state cannot be classified as near to axisymmetric expansion turbulence.

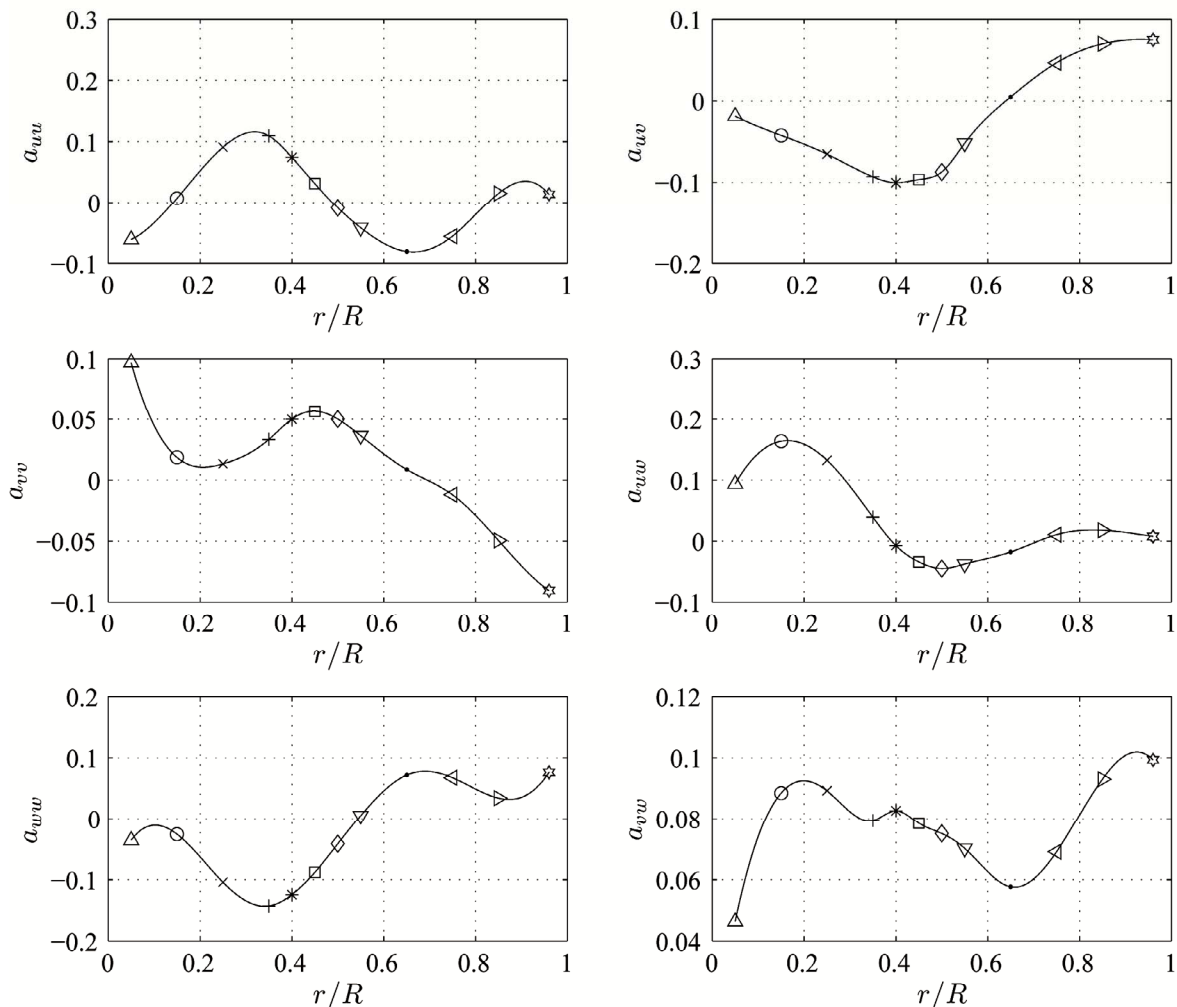


Figure 6. Distributions of Reynolds stress anisotropy tensor components

Moreover, component λ_2 is 376% larger than λ_1 . This important fact is neglected in the AIM (Figure 7) since the anisotropy state is located near the right curve. This same state is equally distanced from left and right line in the BM (Figure 8). It seems that the BM is more sensitive to difference between anisotropy tensor components, which results with better graphical interpretation than the AIM.

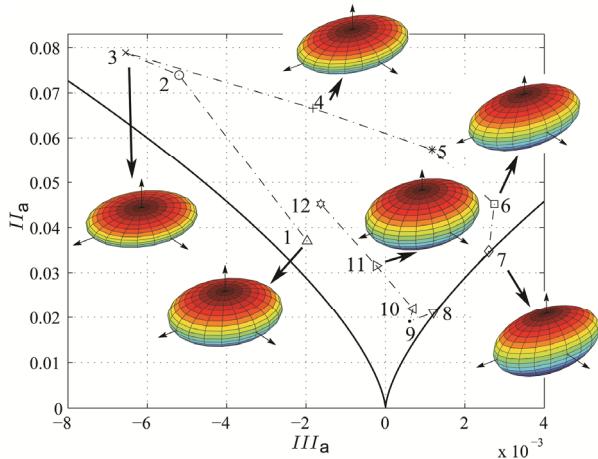


Figure 7. Anisotropy invariant map with ellipsoid shapes formed by Reynolds stress tensor in turbulent swirl flow. Numbers in figure denote measuring positions: 1, $r/R=0.05$; 2, $r/R=0.15$; 3, $r/R=0.25$; 4, $r/R=0.35$; 5, $r/R=0.40$; 6, $r/R=0.45$; 7, $r/R=0.50$; 8, $r/R=0.55$; 9, $r/R=0.65$; 10, $r/R=0.75$; 11, $r/R=0.85$; 12, $r/R=0.96$

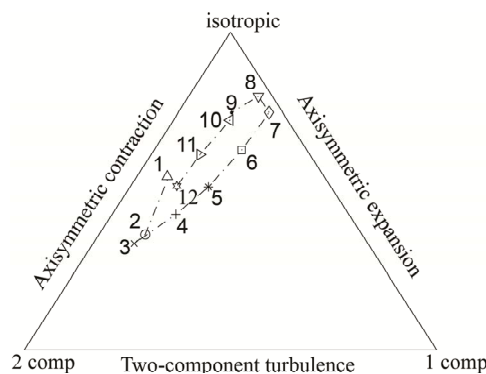


Figure 8. Barycentric map in turbulent swirl flow. Numbers in figure denote measuring positions as in Figure 7

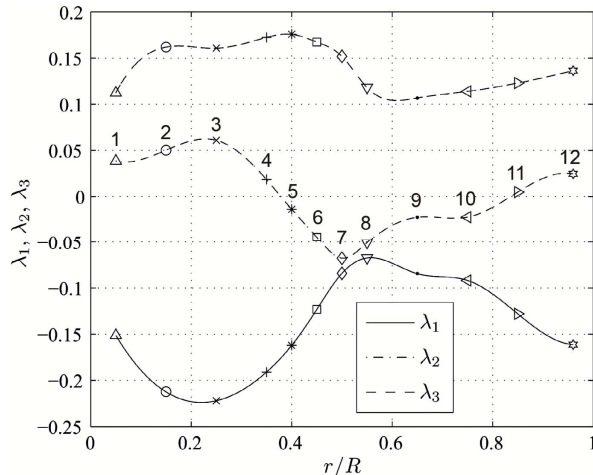


Figure 9. Distribution of principal values of anisotropy tensor. Numbers in figure denote measuring positions as in Figure 7

The AIM (Figure 7) shows that the nearest state to isotropy is at $r/R = 0.65$ (number 9 in Figures 7, 8 and 9), while the BM (Figure 8) gives different visual impression that the nearest state to isotropy is at $r/R = 0.55$ (number 8 in Figures 7, 8 and 9). We cannot make clear conclusion which map shows better the real state in this case because the differences between principal anisotropy components are small at $r/R = 0.55$ and $r/R = 0.65$, which can be seen from Figure 9.

Lumley [1] introduced parameter J to distinguish isotropic from two-component turbulence. The vanishing of this parameter ($J = 0$) indicates two-component state but in the case of isotropic turbulence this parameter becomes unity ($J = 1$). This parameter can be expressed using anisotropy invariant coordinates as

$$J(II_a, III_a) = 1 - 9\left(\frac{1}{2}II_a - III_a\right),$$

but can also be expressed as a function of coefficients used in the BM

$$J(C_{1c}, C_{2c}) = 1 - (C_{1c} + C_{2c}).$$

Figure 10 shows radial distribution of parameter J calculated in these two ways.

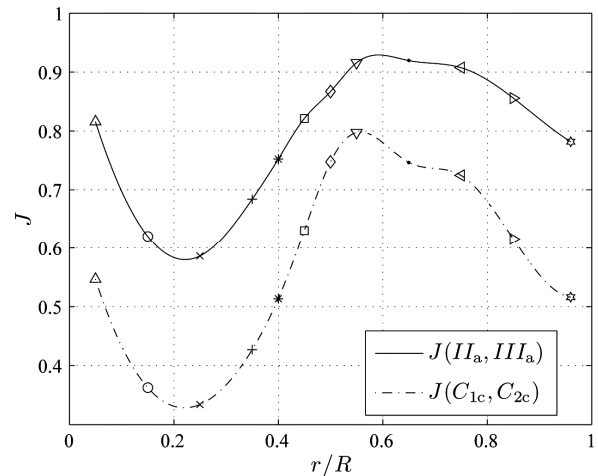


Figure 10. Distribution of parameter J calculated in different ways

Similar trends for these two curves are observed, with the difference that the all anisotropy states that parameter $J(II_a, III_a)$ describes are closer to isotropy than the corresponding states that parameter $J(C_{1c}, C_{2c})$ describes. That means that curve $J(C_{1c}, C_{2c})$ calculated with coefficients which are linear functions of Reynolds stresses has a sharper criterion of isotropy than the curve $J(II_a, III_a)$ calculated with anisotropy invariant coordinates which are nonlinear function of Reynolds stresses.

5. CONCLUSIONS

Anisotropy invariant map (AIM) and barycentric map (BM) were used in order to evaluate anisotropy of

turbulence. Experimental data were utilised to investigate differences between these two maps. It is shown that swirl significantly changed the anisotropy of turbulence. Different states of anisotropy corresponded to different parts of flow regions: points in vortex core were close to axisymmetric contraction state, points in shear layer tended towards axisymmetric expansion state with radius increase and points in mean flow region were parallel to axisymmetric contraction state. Comparing of the same anisotropy states in the AIM and BM indicates that the BM provides better visual interpretation than the AIM, when anisotropy state is close to axisymmetric expansion line in the AIM. Anisotropy invariants (II_a, III_a) are nonlinear functions of anisotropy tensor components while coefficients used in forming of BM are linear functions of principal anisotropy tensor components. This is the reason why differences are observed in these two maps.

ACKNOWLEDGMENT

The authors of this paper wish to express special gratitude to Prof. Dr.-Ing. Svetislav M. Čantrak, for all the knowledge and support that he provides to us, making our steps on the path of science much more secure.

This work is supported by the Ministry of Education and Science of the Republic of Serbia, projects TR 35046 and TR 33048, which we gratefully acknowledge.

REFERENCES

- [1] Lumley, J.L.: Computational modeling of turbulent flows, *Advances in Applied Mechanics*, Vol. 18, pp. 161-178, 1978.
- [2] Keirsbulck, L., Labraga, L. and Haddad, M.: Influence of blowing on the anisotropy of the Reynolds stress tensor in a turbulent channel flow, *Experiments in Fluids*, Vol. 40, pp. 654-662, 2004.
- [3] Oyewola, O., Djenidi, L. and Antonia, A.: Influence of localised wall suction on the anisotropy of the Reynolds stress tensor in a turbulent boundary layer, *Experiments in Fluids*, Vol. 37, pp. 187-193, 2004.
- [4] Lumley, J.L. and Newman, G.: The return to isotropy of homogeneous turbulence, *Journal of Fluid Mechanics*, Vol. 82, pp. 161-178, 1977.
- [5] Banerjee, S., Ertunc, O. and Durst, F.: Anisotropy Properties of Turbulence, in: *Proceedings of the*

13th WSEAS International Conference on APPLIED MATHEMATICS (MATH'08), 15-17.12.2008, Puerto De La Cruz, pp. 26-57.

- [6] Chang, F. and Dhir, V.K.: Turbulent flow field in tangentially injected swirl flows in tubes, *International Journal of Heat and Fluid Flow*, Vol. 15, No. 5, pp. 346-356, 1994.
- [7] Burazer, J., Lečić, M. and Čantrak, S.: On the Non-Local Turbulent Transport and Non-Gradient Thermal Diffusion Phenomena in HVAC Systems, *FME Transactions*, Vol. 40, No. 3, pp. 119-126, 2012.
- [8] Jovanović, J.: *The Statistical Dynamics of Turbulence*, Springer, Berlin Heidelberg New York, 2004.
- [9] Čantrak, S.: Experimental Investigation of Statistical Properties of Turbulent Swirling Flows in Pipes and Diffusers, *Fluid Mechanics and Turbomachines*, 31, pp. 23-66, Karlsruhe, 1982 (in German)
- [10] Simonsen, A.J. and Krogstad, P.A.: Turbulent Stress Invariant Analysis: Clarification of Existing Terminology, in: *15th Australasian Fluid Mechanics Conference: Clarification of Existing Terminology*, 13-17.12.2004, The University of Sydney, Sydney, pp. 26-57.

АНАЛИЗА АНИЗОТРОПНОСТИ ТУРБУЛЕНТНОГ ВИХОРНОГ СТРУЈАЊА

Дарко Р. Раденковић, Јела М. Буразер, Ђорђе М.
Новковић

У раду су примењене две врсте инваријантних мапа како би се проценио степен анизотропности турбулентног вихорног струјања. Коришћене су инваријантна мапа, коју су предложили Ламли и Њуман, као и барицентрична мапа. Анализиране су разлике у визуелном представљању стања анизотропности и изведене су математичке основе за обе мапе. Анализом експерименталних података је показано да постоји значајан утицај вихора на анизотропност турбуленције. Коришћење мапа анизотропности показује да су различите области струјног поља у вихорном струјању окарактерисане различитим стањима анизотропности.